

Field Validated Generic EMT-Type Model of a Full Converter Wind Turbine Based on a Gearless Externally Excited Synchronous Generator

Aramis Schwanka Trevisan ^{ID}, *Student Member, IEEE*, Amgad A. El-Deib, *Member, IEEE*, Richard Gagnon, Jean Mahseredjian ^{ID}, *Fellow, IEEE*, and Martin Fecteau, *Member, IEEE*

Abstract—The integration of wind power plants introduces new dynamics into power systems, forcing reconsiderations of how they are studied, planned, and operated. High quality models are essential to these studies. Manufacturer-specific electromagnetic transient (EMT) wind turbine models are usually available only as black-boxes, which hinders analysis and research. To overcome this issue, this paper proposes a generic EMT-type model for a specific type-IV wind turbine system, which is validated against field measurements from a wind turbine of the same type. More precisely, it proposes a wind turbine model based on an externally excited synchronous generator system connected to a full converter composed of a six-pulse diode rectifier, a dc–dc boost stage and a two-level voltage source converter. The required control features and internal protection schemes are considered and described. Two different fault ride-through control strategies, in line with existing grid codes, are implemented. A corresponding EMT-type hybrid model representation is also developed based on newly proposed switched equivalent circuits and average models for the considered hardware, control, and power electronics stages. It allows for the use of larger simulation time steps, hence considerably improving computation times.

Index Terms—Full Converter Wind Turbine, Wind Power Plants, Power system, Hybrid model, Average model, Switching function model, Real-time application, Field measurements.

Manuscript received July 13, 2017; revised October 16, 2017 and April 19, 2018; accepted June 11, 2018. Date of publication June 26, 2018; date of current version September 25, 2018. Paper no. TPWRD-00926-2017. (*Corresponding author: Aramis Schwanka Trevisan*)

A. S. Trevisan is with the Department of Electrical Engineering, Ecole Polytechnique de Montréal, Montréal, QC H3T 1J4, Canada and with WRD Wobben Research and Development GmbH (ENERCON R&D) in Aurich, D-26607, Germany (e-mail: aramis.schwanka.trevisan@enercon.de).

A. A. El-Deib is with the Electrical Power and Machines Department, Faculty of Engineering, Cairo University, Giza 12613, Egypt, on leave to the University of Science and Technology at Zewail City, Cairo 12588, Egypt (e-mail: aeldeib@zewailcity.edu.eg).

R. Gagnon is with the Hydro-Québec Research Institute (IREQ), Varennes, QC J3X 1S1, Canada (e-mail: Gagnon.Richard2@ireq.ca).

J. Mahseredjian is with the Department of Electrical Engineering Ecole Polytechnique, Montréal, QC H3T 1J4, Canada (e-mail: jean.mahseredjian@polymtl.ca).

M. Fecteau is with the System Studies, Hydro-Québec TransÉnergie, Montréal QC H5B 1H7, Canada (e-mail: Fecteau.Martin@hydro.qc.ca).

Color versions of one or more of the figures in this paper are available online at <http://ieeexplore.ieee.org>.

Digital Object Identifier 10.1109/TPWRD.2018.2850848

I. INTRODUCTION

OPERATORS of modern power systems have been integrating inverter-based technologies at a fast pace, spurred on recently by the integration of wind turbines [1]. The increased complexity and new dynamics added by this new equipment are forcing reconsiderations in the way power systems are studied, planned and operated, thus yielding the need for more advanced modeling and analysis methods.

As one consequence, the provision of manufacturer-specific electromagnetic transient (EMT) models has already become a requirement for the connection of new generating units in some grid areas [2]. However, due to confidentiality issues, these models are often provided as black-boxes, thus hindering the access to internal control systems and hardware parameters and, therefore, the use of specific analysis techniques.

To overcome some of these difficulties in specific cases, generic transient stability type models (in phasor domain) have been proposed for different types of wind turbine systems [3]–[6]. Nevertheless, the intrinsic limited frequency bandwidth consideration of these models, as well as typical assumptions for grid model equations in phasor domain, limit the application range of such models.

The present work aims at the development of generic EMT-type models. Several types of studies require the use of EMT models. The EMT-type models are circuit-based and can represent multiphase systems with accurate transmission line models, component nonlinearities, real controller blocks with high-bandwidth components, among others. Reference [7] addresses the need for EMT-type simulations to support the massive integration of wind power plants. Moreover, it also suggests a typical list of EMT-type power system studies to be performed in this context.

In the specific case of wind turbine systems, some previous studies have introduced generic EMT models to represent different types of wind turbines. References [8]–[12] proposed detailed models for type-III (doubly-fed induction generator based) wind turbine systems. Valuable insights into specific full converter systems can also be obtained from references [13]–[17]. Notably, generic EMT-type model representations of types II, III and IV wind turbine systems were addressed in [7], although not to the same level of modeling detail presented in this paper. For example, protection systems and fault

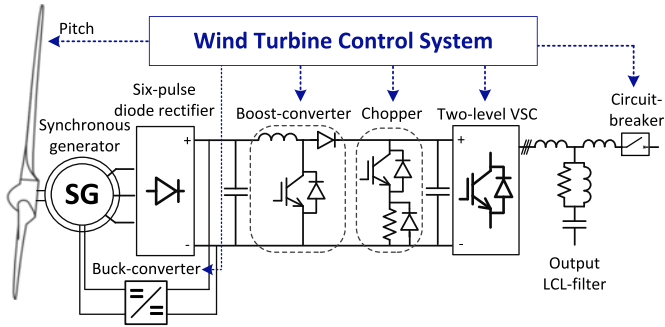


Fig. 1. Wind turbine system to be modelled.

Ride-Through (FRT) strategies were not considered in [7], consequently limiting the applicability of these models in the context of EMT-type power systems studies.

This paper proposes a generic EMT-type detailed model (DM) for a specific type-IV wind turbine hardware topology, illustrated in Fig. 1. It focuses on a system based on a directly-coupled (gearless) externally-excited synchronous generator, which is connected to a three-stage full converter system consisting of a six-pulse diode rectifier, a dc-dc boost converter and an IGBT-based two-level voltage source converter (VSC).

The wind turbine controller is developed and explained. To make the model more generic and facilitate usage, the controls were developed by means of the per-unit system. Hardware and control protection schemes are considered. Additionally, in contrast to the aforementioned previous works [8]–[17], two FRT control strategies were also implemented in the model, which are in line with existing European and North and South American Grid Code requirements ([2], [18]–[21]).

Furthermore, an EMT-type hybrid model (HM) is developed for the same wind turbine system by combining average-value models (AVM) and switched equivalent circuits for the power electronics stages. The HM allows for much larger simulation time-steps under some acceptable assumptions. As a result, faster computation times are achieved, making the HM also suitable for real-time applications.

Finally, field tests were conducted in a real wind turbine of similar type to validate the implemented FRT-strategies and to demonstrate that the proposed generic EMT-type model contains the required level of details to provide sufficiently accurate and adequate performance.

It is important to note that the model development process outlined in the next sections aimed at a 2 MW wind turbine to match the system against which it has been validated with field measurement data. In the context of power system studies, it may be, however, necessary to use this model to represent a wind farm and not a single unit. To achieve this, an additional parameter corresponding to *the number of lumped wind turbine models* is made available for the model user. This parameter basically explicitly defines the number of equal wind turbines to be considered in aggregated manner.

This paper is structured as follows. Section II deals with the mechanical system representation and its control. Section III addresses the grid-side converter controller. In Section IV, emphasis is given to the specific current control type used and to the

design of the LCL-output filter. Two different FRT strategies are presented and implemented in Section V. In Section VI, the HM is developed. Finally, Section VII covers the validation of the proposed system against specific field measurements performed at a wind turbine of similar type. All hardware and control parameters proposed for the generic EMT-type wind turbine model can be found in the Appendix.

II. AERODYNAMIC REPRESENTATION, MECHANICAL SYSTEM AND CONTROL OF THE SYNCHRONOUS MACHINE

The aerodynamic model for the turbine of this paper is based on [22] and uses well-known equations for power extraction from the wind. An analytical expression is used to represent the power coefficient of the turbine, which is a function of the tip-speed ratio and the blade pitch angle.

The wind turbine rotor is assumed to be directly coupled (no gearbox) to the rotor of the synchronous machine (SM). Furthermore, the blade system and the machine rotor are assumed to lie on the same plane, allowing a single-mass type of mechanical system representation. Additionally, the three-phase stator system of the SM is directly connected to a six-pulse diode bridge rectifier, as illustrated in Fig. 1.

It is worth mentioning here that, in the context of industrial applications of wind turbines, the directly-coupled nature of the turbine-generator system yields some specific requirements for these components. Some of these affect, for example, the electrical and mechanical design of the synchronous machine resulting in the use of a large number of pole pairs and unusual proportions. As a result, electrical parameters may differ from typical values in other applications.

From a control perspective, different controllers could be conceived for the electromechanical system described above, depending on the primary objectives, pre-defined control requirements and existing hardware constraints. For the purposes of this work, a maximum power tracking requirement is assumed. This means, given a certain wind speed, the system is expected to extract the maximum power possible from the wind and operate at an optimal condition.

Due to the directly-coupled nature of the wind turbine system, the optimal SM rotor rotational speed ω_r is the one that maximizes the turbine mechanical power extraction from wind $P_{m,turb}$. In other words, for each wind speed v_{wind} there is an optimal ω_r value for the SM. Fig. 2 illustrates this.

Since a six-pulse diode bridge rectifier is connected to the stator side of the SM, this work assumes that the SM excitation is used to control the rotor speed ω_r . To reduce controller efforts, the optimal rotor speed reference $\omega_{r,ref}$ is first filtered. The error between the filtered reference and the measured rotational speeds, $\omega_{r,ref,filt}$ and $\omega_{r,meas}$ respectively, is sent as input to the excitation controller, which is of proportional integration (PI)-type with dynamic limitations and anti-windup capability. The upper and lower limiters are used to represent the real voltage constraints imposed by the dc-link voltage V_{DC1} , to which the buck-converter is connected. A PWM-generator is used to convert the controller output into gating signals, which are then applied to the buck-converter to generate the required SM excitation voltage.

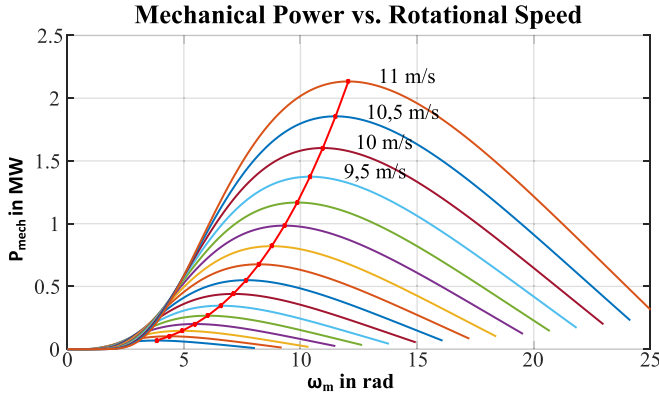


Fig. 2. Mechanical power vs. rotation speed for different wind speeds (in steps of 0.5 m/s). Optimal rotor rotational speeds are also being indicated in red.

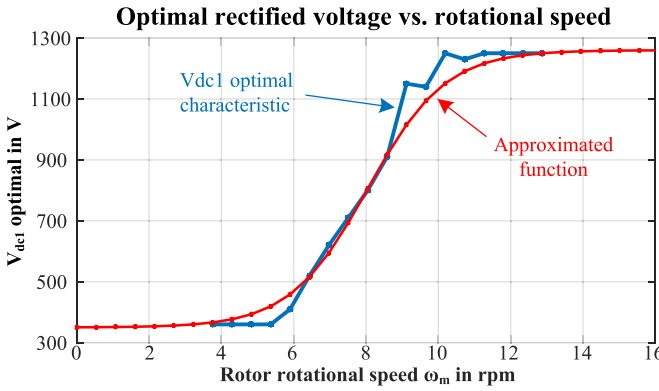


Fig. 3. In blue: V_{DC1} versus ω_r characteristic for maximum power extraction. In red: approximated function.

Additionally, it is important to note that the rectified dc-link voltage can be understood as a further degree of freedom for the system considered above (synchronous machine connected to a diode rectifier). In that sense, it is further used to help the system comply with the maximal power tracking requirements and is used in this work for power losses minimization in the turbine-generator system. In other words, for each ω_r there is an optimal combination of excitation voltage V_{SG_field} and rectified voltage V_{DC1} . For the proposed model, this characteristic was extracted through simulation-based scanning and the result is illustrated in blue in Fig. 3. It is assumed, as further explained in Section III, that the grid-side converter controls V_{DC2} , the second dc-link voltage, to a constant value of 1250 V.

The characteristic illustrated in Fig. 3 is used as the base for the boost-converter controller. For its implementation in the model, an approximated function was obtained through polynomial fitting. The resulting function is also illustrated in red in Fig. 3. It is then further used to generate the boost-converter duty-cycle d_{boost} given the measured rotor speed.

Finally, an overview of the buck- and boost-converter controller structures, which lead to the generation of the pulse signals, is depicted in the next Fig. 4.

At this stage it is important reinforce that the model development process aimed at a 2 MW wind turbine to match the system against which it has been validated with field mea-

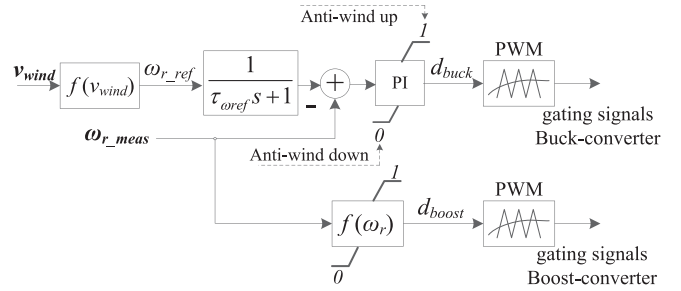


Fig. 4. Buck and boost-converter controller topologies.

surement data. Although the controller development and the hardware parameters are made available in the per-unit system, changes in the turbine rating resulting from a direct downscaling or upscaling of the system parts are prone to yield non-realistic components and/or operating conditions. This is mostly due to the directly-coupled and variable-speed nature of the turbine-generator system. To exemplify one of the possible issues, it suffices to observe that larger wind turbines, with larger rotor diameters, tend to have lower rotational speeds to reduce mechanical stress. For the wind turbine system considered here, depicted in Fig. 1, lower rotational speeds are likely to yield some modifications in the turbine-generator system, such as different blade profiles and the number of generator pole pairs, that are not inherently changed through an upscaling by means of a simple definition of new ratings in the per-unit system. For the specific case in which larger generating units are needed for power system studies, it is advisable to use the model parameter discussed in Section I, since it explicitly address a lumped (i.e., aggregated) representation of wind turbine models.

III. GRID-SIDE CONVERTER CONTROL

The use of full converter systems offers several advantages [22]–[24]. Its application in wind turbines allows for fast separate control of active and reactive currents, among others. Such capabilities are very valuable when it comes to grid support services [25]–[28].

In the proposed wind turbine system, the output active and reactive current components of the grid converter are used to control the second dc-link voltage V_{DC2} and the reactive power being injected into the grid, respectively.

The active current component is controlled by the dc-link controller, which is designed to maintain V_{DC2} at a constant value of 1250 V. This value was chosen to meet the main performance requirements considering a phase-to-phase ac output terminal voltage of 690 V and imposed by the chosen current control type (see Section IV). A controller of PI-type with dynamic limitations and anti-windup capability is used. The negative error between the reference value V_{DC2_ref} and the filtered measured value of V_{DC2} , further referred to as V_{DC2_filt} , is used as input. During normal operation, the upper controller limit is defined by the maximal acceptable converter current (i_{max}), which is a model parameter and should take hardware constraints into account. In case of FRT operation, however, the upper limit value can change depending on the FRT strategy in use and its settings

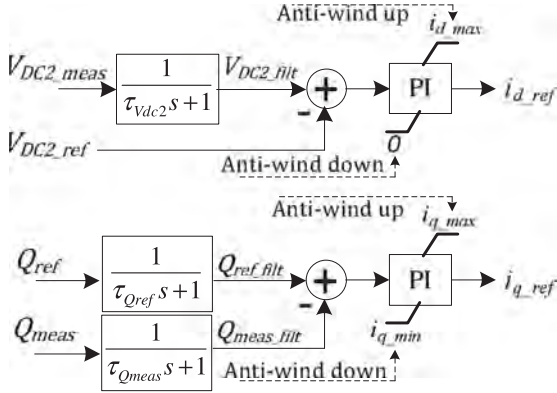


Fig. 5. DC-link and reactive power controller topologies.

(see Section IV). The lower limit is simply defined as zero, since it is assumed that the active power flow is always towards the grid.

The reactive current component is controlled to follow a reactive power reference Q_{ref} . Again, a controller of PI-type with dynamic limitations and anti-windup capability is used. Its input is the error between the filtered value of Q_{ref} and the measured reactive power at the turbine terminals Q_{meas} , referred to as Q_{ref_filt} and Q_{meas_filt} , respectively. During normal operation, priority is given to the active current component and the upper and lower controller limits are dynamically calculated under the consideration of the active current reference, i_{d_ref} , and maximal acceptable converter current i_{max} . Consequently, the reactive current component might be limited to meet the maximal current constraint imposed by i_{max} . Finally, it is important to note again that this can change during FRT-operation, since, depending on the chosen FRT-Strategy, priority can be given to the reactive current. If this is the case, it is the active current component that can be limited so to comply with the maximal acceptable converter current i_{max} (see Section IV). The topologies for the dc-link and reactive power controllers are illustrated in Fig. 5.

IV. CURRENT CONTROL AND OUTPUT FILTER DESIGN

A two-level IGBT/Diode based topology was considered for the VSC system. Moreover, a hysteresis-band current control (HCC) type is assumed. This choice was mostly based on the robustness and high speed of response of the HCC and because it is a generic model, which also allowed for acceptable results in the comparison with field tests (discussed later in Section VII). However, it is important to emphasize here that a model-based design approach was applied to the development of the proposed EMT-type wind turbine model in this work and, therefore, if required, the HCC could be replaced by another type of current controller, e.g., a proportional resonant (PR) controller or a PI current controller with decoupling of the d and q axis and feed-forward of filter voltages. Nevertheless, if modifications are made, it is advisable to investigate for further required changes to properly accommodate the new controllers (output filter design, second dc-link voltage control, among others).

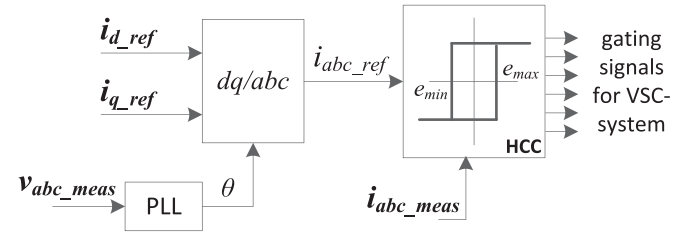


Fig. 6. Implemented HCC scheme for VSC system.

Bode Diagram of Output Filter

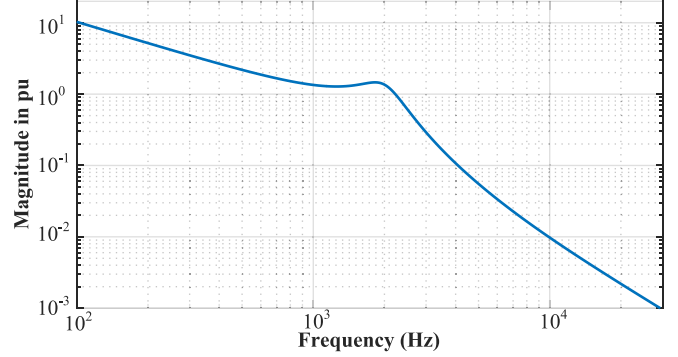


Fig. 7. Bode diagram of grid-converter LCL output filter.

Fig. 6 depicts an overview of the HCC. The dq reference currents sent by the grid-side converter controllers (see Section III) are transformed into the abc -frame by using a dq/abc -transformation with the reference angle θ extracted from the measured voltages v_{abc_meas} at the turbine terminals through a phase-locked loop (PLL) system, as used in [13].

Furthermore, an LCL-type output filter is employed. The detailed filter topology can be extracted from Fig. 1. It is designed to comply both with a maximum switching frequency and with some pre-defined power quality requirements. An additional RL parallel damping circuit, as presented in [29], is also considered. Valuable insights and important filter design considerations can be extracted as well from [30] and [31]. The filter was designed to have its resonance frequency at 2 kHz, from which an attenuation rate of -60 dB/dec is expected. Its frequency characteristic is illustrated in the bode diagram presented in Fig. 7.

V. FRT-CONTROL STRATEGIES AND PROTECTION

Two different FRT control strategies were implemented in the proposed model, based on existing grid-code requirements in different countries ([2], [18]–[21]). Their main characteristics are illustrated in Fig. 8.

FRT-Mode 1 is to be used when grid support in form of additional reactive current injection during under-voltage ride-through (UVRT) and overvoltage ride-through (OVRT) events is required. In this case, an additional reactive current setpoint proportional to the voltage deviation is sent to the grid-side converter. More precisely, this additional current, defined in per unit, is calculated by the multiplication of the voltage deviation, also in per unit, with a pre-specified proportional factor times the converter rated current. Different proportional factors k_{uvrt} and

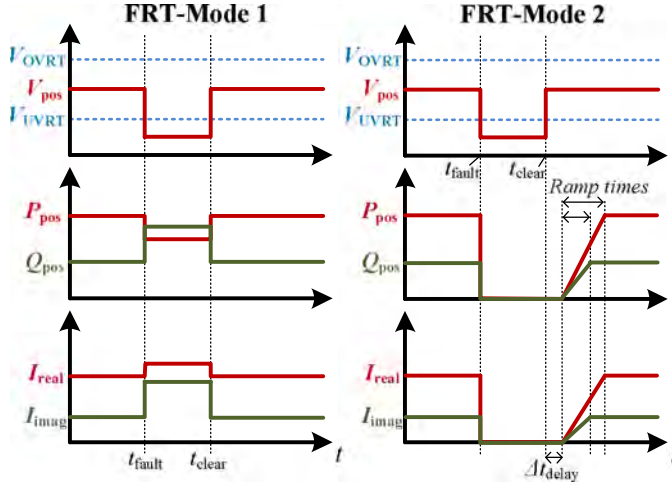


Fig. 8. FRT strategies implemented in the model.

k_{ovrt} can be set for UVRT and OVRT, respectively. Moreover, FRT-Mode 1 gives priority to the reactive current component so that, depending on the severity of the fault and on the values set for k_{uvrt} and k_{ovrt} , the active current component might be limited, or even reduced, to allow for the required reactive current injection while not exceeding the maximum current limit i_{max} provided for the VSC system. This explains the slightly reduction observed in the active power for the FRT-Mode 1 illustrated in Fig. 8.

FRT-Mode 2 differs from the previous one in the sense that, once an FRT event is detected, the wind turbine stops its active and reactive power injection and remains connected to the grid. This is done by forcing the active and reactive current set points to zero. Once the turbine detects that the voltage has recovered, it ramps back its current reference values respecting separate pre-defined ramp rates for both active and reactive components. Furthermore, time delays can be set separately for the initialization of the ramps. Among other applications, this last feature can be used to allow for a first stabilization of voltage after fault clearance through reactive current injection, before reinjection of active current into the grid.

A braking-chopper system is connected in parallel to the second dc-link to avoid overvoltages, reduce the stress on hardware components and, therefore, protect the equipment during faults. Independent of the FRT-mode used, a maximal FRT-time is to be set in the model to account for real hardware constraints. If this time is exceeded, an opening signal is sent to the three-phase breaker connected at the turbine terminals, as shown in Fig. 1, disconnecting it from the grid.

A secondary protection level is also implemented in the model. It accounts for the maximum and minimal acceptable values for voltage and frequency for the hardware system. Each of these triggers is to be set with a respective action time delay to allow for the compliance of different Grid Code requirements. Voltages and frequency are, therefore, constantly monitored by the wind turbine control system. Whenever one of the voltage or frequency protection conditions is met for its corresponding action time delay, an opening signal is sent to a three-phase

breaker at the turbine terminals, consequently separating the wind turbine from the grid.

VI. HYBRID MODEL IMPLEMENTATION

Simulations with the DM representation require a small numerical integration time-step to allow for proper solution of the switching characteristics of the power electronics devices. Nevertheless, depending on the focus of the required studies, the use of average models and switched equivalent circuits, based on switching functions [24], can be very powerful, since they can allow for the use of larger simulation time-steps, consequently improving computation times of simulations. This can be very useful, for example, for simulation of large-scale power systems as well as for real-time applications. The hybrid model (HM) representation developed in this work aimed at the use of a simulation time-steps as large as $50 \mu s$.

The full converter system developed in the previous sections contains different power electronics stages to be considered in the HM development. Of all these stages, only the diode bridge rectifier is left in its original DM representation in the HM. This is due to the expected low frequency diode transitions resulting from the low frequency ac stator voltages of the direct coupled synchronous generator.

On the other hand, an AVM representation was chosen for the buck-converter system. It was developed based on [29] and assumes an averaging of the high frequency components. Thus, the value of the rectified generator voltage V_{DC1} is multiplied with the given buck duty-cycle d_{buck} to directly generate the excitation voltage V_{SG_field} , which is one input of the SG model. Furthermore, to continue to still properly take into account the excitation power drained from the dc-link and in accordance with the AVM development principles in [29], the primary side of the buck-converter is represented as a controlled current source connected in anti-parallel to the rectified generator voltages. Its reference value corresponds to the actual generator field current multiplied by the duty-cycle d_{buck} .

In contrast to the buck converter, a so-called switching function model was preferred for the boost converter instead of an AVM representation. There are two main reasons for this choice. First, high frequency current dynamics through the boost-converter reactor, which can impact the dc-link voltage and, therefore, the fast inner loops of grid-side converter controller, are considered. Secondly, the switching function representation also allows for the consideration of the discontinuous conduction mode of the boost converter, which is not the case for an AVM representation. The implemented switching function model is based on [32] and is illustrated in Fig. 9. The PWM-averaging block is explained later in this section.

To elucidate the working principle of the switching function model of the boost-converter, two cases are considered. If the received gating signal is 1 (boost-converter IGBT is in conduction mode), the measured boost reactor current i_{boost} is sent as a reference value to the controlled current source and is, therefore, completely drained by it. To guarantee a zero voltage (short-circuit) at the secondary side of the diode, the measured value of the second dc-link V_{DC2_meas} is sent to a controlled voltage

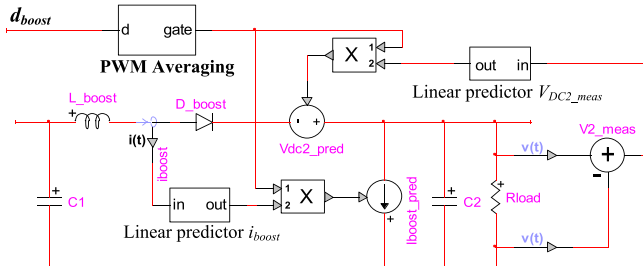


Fig. 9. Switching function model of the boost circuit.

source. If the gating signal is equal to zero (IGBT is blocked), then both controlled sources receive zero references and can be neglected in the circuit analysis.

Moreover, to avoid numeric algebraic loops in the simulation and, thus, to make the HM more suitable for real-time applications (since solver iterations are avoided), the measured values i_{boost} and $V_{DC2,meas}$ are sent to the sources through a so-called linear predictor block. It linearly estimates the actual solution y_k^* for the measured values by considering the last two simulation solutions, y_{k-1} and y_{k-2} , respectively. This assumption is acceptable, since the current through the boost reactor and the voltage over the second dc-link capacitor are neither expected to change quickly nor have any discontinuities. The use of the linear-predictor blocks results in negligible error in these cases and is, therefore, more suitable than the use of first-order delay blocks.

It is important to emphasize that the proposed switching function representation for the boost-converter allows for gate firing signals values between 0 and 1. This is due to the use of controlled voltage and current sources instead of standard IGBT models, which would inherently accept only 0 or 1 as gating signals. One of the main advantages of this property is the fact that gating signals values between 0 and 1 can be further used to obtain an almost precise representation of the switching characteristics, even under the use of larger simulation time-steps.

To exemplify the issue described above related to the use of large simulation time-steps in EMT-type simulation of power electronics, let us assume the direct use of the desired time-step of $50\ \mu s$ in conjunction with the DM representation of a boost converter. Since the gating signals are converted from duty-cycle values by sawtooth or triangle function based PWM generators, the conversion precision is strongly dependent on the integration time-step used in the simulation environment. In the DM representation, the PWM generators have a carrier frequency of 2 kHz. This value, combined with a simulation time-step of $50\ \mu s$, only allows for 10 simulation results within a switching period. One direct consequence would be a duty-cycle precision of only 10%.

To overcome this issue, a special triangle function based PWM generator was developed and will be further referred to as PWM-averaging. It is capable of considering the precision error resulting from the use of a larger simulation time-step and of automatically correcting it by the end of every switching period by sending a gating signal with a value between 0 and 1. This capability is illustrated in the upper diagram of Fig. 10: in

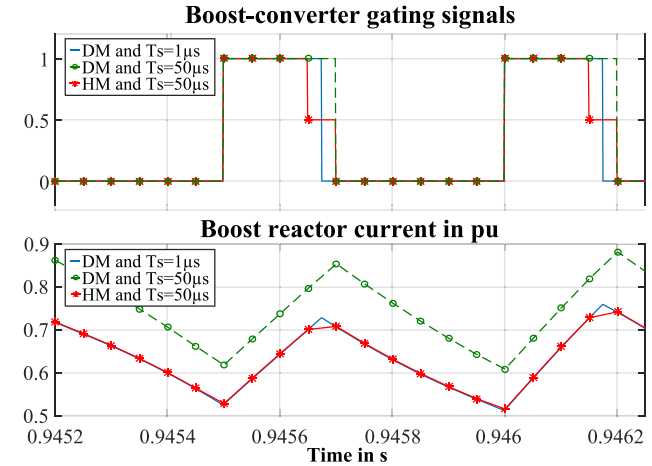


Fig. 10. Boost simulation comparison: i) blue: DM with time-step $T_s = 1\ \mu s$; ii) green: DM with $T_s = 50\ \mu s$; iii) red: HM with $T_s = 50\ \mu s$.

blue, the gating signal generated by a standard triangle-function based PWM-generator simulated with a time-step of $1\ \mu s$; in green the gating signal for the same block, this time calculated with a time-step of $50\ \mu s$; and, in red, the resulting gating signal characteristic from the new PWM-averaging also simulated with a $50\ \mu s$ time-step.

As shown in Fig. 10, a sufficiently good representation of the gating signal generation is not possible without the use of the PWM-averaging technique if a simulation time-step of $50\ \mu s$ is used. This is due to the expected 1-to-0 IGBT-transitions occurring between two simulation results and the resulting poor duty-cycle resolution achieved with $50\ \mu s$ integration time-steps. Consequently, the poor duty-cycle resolution affects the boost-converter reactor current, which can now be under- or over-estimated, depending on the case. This phenomenon is illustrated in the lower diagram of Fig. 10. It shows that, aside from the correction step at the end of each switching period, an almost perfect match can be obtained for the boost-reactor current between the DM model simulated with a time-step of $1\ \mu s$ and the HM representation (considering the PWM-averaging technique), although a 50 times larger time-step is used for the latter case.

The PWM-averaging technique discussed above is also used to support the development of a switching function representation for the chopper stage. Again, a switched equivalent circuit representation is preferred over an AVM due to the possible consideration of higher frequency components in the chopper current, when it operates. This is important, since the chopper operation has a direct impact on the second dc-link voltage V_{DC2} , which is controlled through the active current component of the grid-side converter system (see Section III). Simplifications at this stage could, therefore, affect the currents injected into the grid.

The implementation of the switched equivalent circuit for the chopper stage in the HM representation is done by simply replacing its power electronics DM circuit by a controlled current source connected in anti-parallel to the dc-link capacitor. The set point value for this current source is given by the multiplication

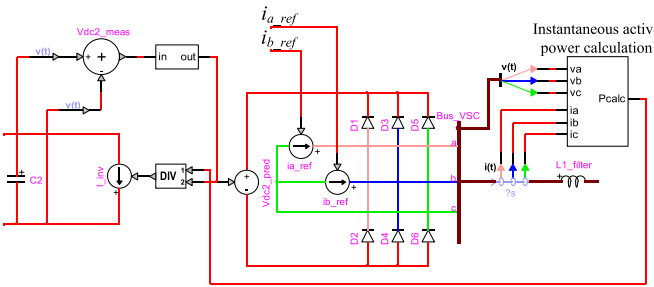
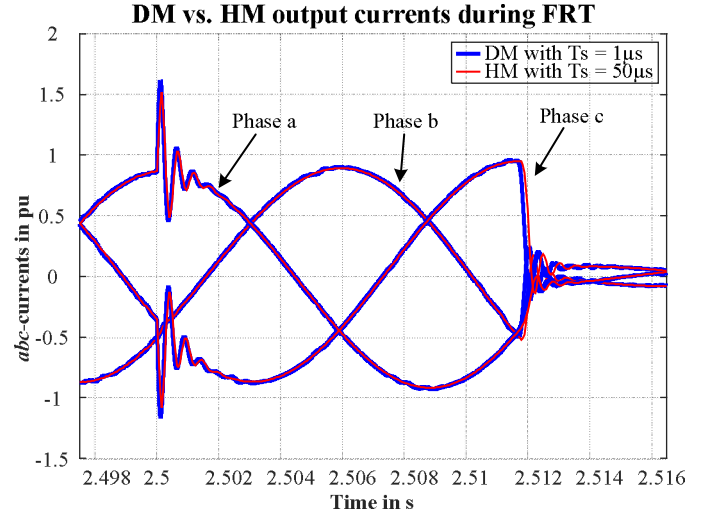


Fig. 11. AVM of a HCC based VSC-system.

of the chopper gating signal, coming from the PWM-averaging block, with a current value, which is calculated by dividing the measured dc-link voltage by the value of the chopper resistance. It is also important to note that the chopper IGBT conduction losses are considered by adding its equivalent resistance value to the chopper resistance.

Finally, an AVM representation for the grid-side converter is proposed. Due to the main characteristics of the HCC-based VSC-system (see Section IV), the VSC-system is further modelled as two star-connected ungrounded current sources injecting the reference currents into phases *a* and *b*. A third current source feeding into the phase *c* is not needed, since the VSC-system is represented by a star-connected ungrounded circuit and, therefore, only the injection of two reference currents is required. Moreover, to continue to still take the effect of the anti-parallel diodes of the VSC-system into consideration, these are further represented as connected to the output of the controlled current sources, forming a diode-rectifier system leading to a controlled voltage source. This source receives the linearly predicted measured value of the second dc-link V_{DC2_meas} as set point during simulation. It is important to note that keeping this diode representation form in the AVM representation is important for two reasons: i) it avoids any numerical overvoltages at the controlled current source nodes resulting from a series connection of these sources to the inductive elements of the LCL output filter, transformer and grid; and ii) it can still build a path for currents back to the second dc-link capacitor in case of sustained overvoltages at the grid side.

To complete the AVM representation of the VSC-system, an anti-parallel current source is connected to the secondary dc-link capacitor. It allows for power balance maintenance in the HM representation by considering the active power injected into the grid and discharging the dc-link capacitor accordingly. For this, the instantaneous active power injected into the grid is measured and divided by the linearly predicted measured value of V_{DC2_meas} to generate the current set point for the controlled current source. Again, the predictor block is used to avoid the creation of numeric algebraic-loops in the simulation. As explained above for the case of the boost-converter HM model, the use of the predictor block avoids solver iterations, improving computation time and, therefore, making the model more suitable for real-time applications. The final representation of the HM representation of the HCC based VSC-system is given in Fig. 11.

Fig. 12. Terminal currents: DM ($T_s = 1 \mu s$) vs. HM ($T_s = 50 \mu s$).

Finally, to prove the efficiency of the proposed HM representation for the wind turbine system, its results were benchmarked against DM simulation results. A sudden voltage drop from 1 to 0.7 pu is simulated under FRT-Mode 2 operation. The wind turbine terminal *abc*-currents into the grid are compared and illustrated in Fig. 12. It is possible to see a very good match between DM and HM models although a 50 times larger simulation time-step is used for the HM representation.

VII. PERFORMANCE VALIDATION AGAINST FIELD TESTS

To benchmark the performance of the proposed generic EMT-type wind turbine system, the model was validated against field tests performed on a turbine of similar type.

The tests were performed in one turbine of the 365 MW Seigneurie de Beaupré wind power plant (WPP), in Québec, Canada. This WPP is composed of a 34.5 kV 60 Hz underground collector system with 164 wind turbines. A so-called short-circuit container, similar to the one used in [33], was connected in series with an ENERCON E-82 2.3MW turbine. It allowed for the application of different faults with different residual voltages directly at the turbine terminals.

To reduce the disturbance as seen from the grid, the short-circuit container makes use of a bypass-breaker that automatically opens around two seconds before and closes two seconds after the fault application. By doing so, a high inductive element is added between the fault and grid during the tests.

The grid representation has been developed based on the short-circuit capacity and the X/R relation of 340MVA and 3.1, respectively, provided for the terminals of the turbine without the consideration of the short-circuit container.

Due to space limitations, only four of the performed FRT field tests are illustrated here. The validation in this study is based on positive sequence values for the terminal voltage V_{pos} , and the measured three-phase active and reactive powers for the fundamental frequency, P_{pos} and Q_{pos} , respectively.

Moreover, it is important to note that the wind turbine model proposed in this paper is generic and does not account for real

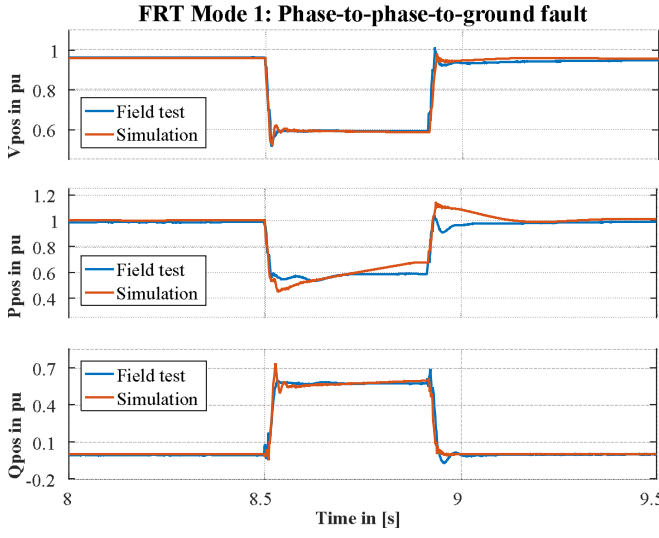


Fig. 13. Field test (blue) vs. simulation (red) results for a phase-to-phase-to-ground fault in FRT-Mode 1 with $k_{uvr} = 3$.

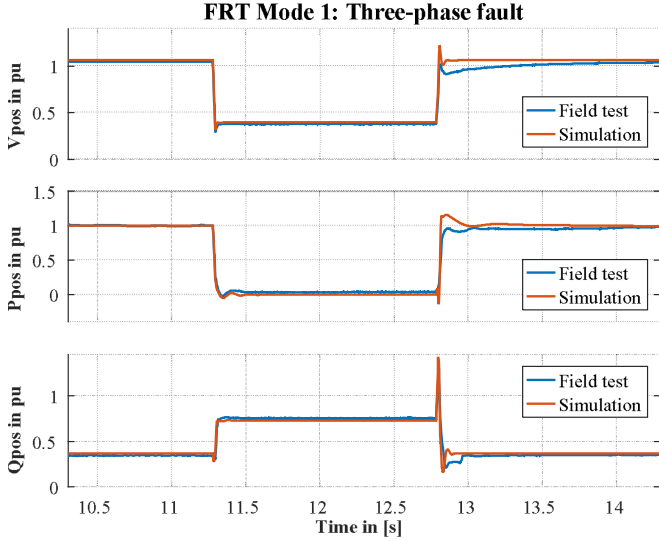


Fig. 14. Field test (blue) vs. Simulation (red) results for a three-phase fault in FRT-Mode 1 with $k_{uvr} = 3$.

turbine parameters and controllers. For this reason, no perfect match between measurement and simulations is to be expected. The goal of this validation is to demonstrate that the proposed generic EMT-type model is sufficiently accurate and provides adequate performance when compared to field tests of a real wind turbine of the same rating and similar type.

FRT Mode 1 was tested with a proportional factor of k_{uvr} equal to 3, which defines the amount of additional reactive current during FRT operation (see Section V). Fig. 13 and Fig. 14 illustrate the comparison between the real turbine and the proposed model responses to a phase-to-phase-to-ground and a three-phase-to-ground fault, respectively.

Similar tests were performed to validate the FRT-Mode 2 strategy implementation. The real turbine and proposed model

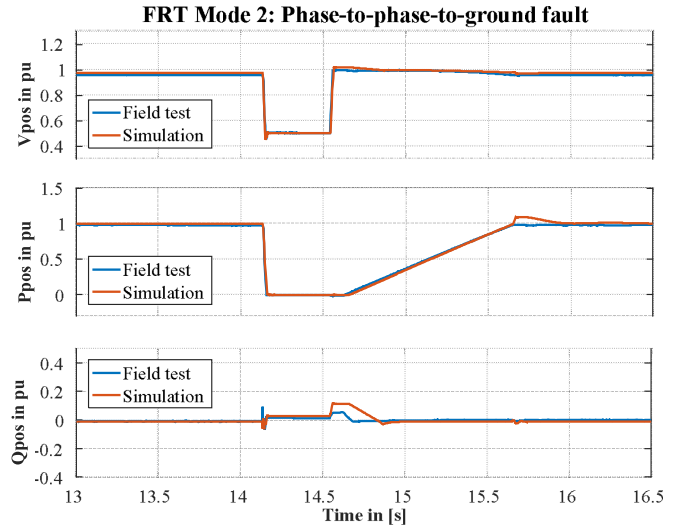


Fig. 15. Field test (blue) vs. Simulation (red) results for a phase-to-phase-to-ground fault in FRT-Mode 2.

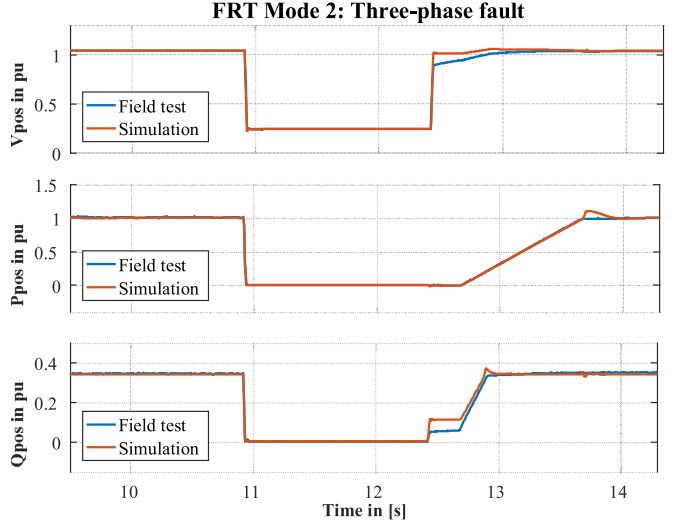


Fig. 16. Field test (blue) vs. Simulation (red) results for a three-phase fault in FRT-Mode 2.

responses for two-phase-to-ground and three-phase-to-ground faults are illustrated in Fig. 15 and Fig. 16, respectively. Also, a time delay of 100 milliseconds was used in the start of the active and reactive power ramps after fault clearance.

As illustrated in Fig. 13 to Fig. 16, although a good match is achieved between the proposed model and the results from field measurements, it is still possible to note some differences, for example, at fault clearance. Part of these deviations are due to the simplified grid representation used, which, due to lack of available information, did not account for the detailed WPP collector system representation. The other part of these differences can be attributed to the proposed wind turbine model and could possibly still be reduced in a case-by-case tuning of generic parameters and controllers used. However, it is important to note

TABLE I
WIND TURBINE c_p (λ , β)-CHARACTERISTIC (BASED ON [22])

c_1	c_2	c_3	c_4	c_5	c_6	c_7	c_8	c_9
0.2065	200	0.15	0.05	2.14	13.2	13	-0.02	-0.003

TABLE II
WIND TURBINE RATED VALUES

Parameter	Name	Value	Unit
R_rotor	Wind turbine rotor radius	42	m
lambda_opt	Optimal tip-speed ratio	7.1	-
Vspeed_nom	Nominal wind speed	11	m/s
Vspeed_in	Cut-in wind speed	3.5	m/s
U_rated	Phase-to-phase rated voltage	690	V
P_rated	Rated active power	2	MW
Q_rated	Rated reactive power	1.5	MVar
i_max	Maximal acceptable converter current	3180	A
f_buck	PWM carrier-freq. of buck converter	2000	Hz
f_boot	PWM carrier-freq. of boost converter	2000	Hz
f_chopper	PWM carrier-freq. of braking chopper	2000	Hz
Vdc_ref	Vdc2 reference voltage value	1250	V

that the proposed EMT-type model is not manufacturer-specific and, therefore, does not account for the actual wind turbine parameters and controllers. Therefore, a perfect match between field tests and simulations results is not possible and was not expected.

VIII. CONCLUSIONS

This work proposes a generic EMT-type model for a specific type-IV wind turbine hardware topology. More specifically, the system considers a gearless externally excited synchronous generator and a three-stage full converter composed of a passive rectifier, a dc-dc converter and a two-level VSC.

All main components and controller topologies were developed, characterized and explained. Two different FRT control strategies were implemented, covering a large list of Grid Code requirements worldwide. Moreover, hardware and control protection schemes were also taken into account.

Two different EMT-type model representations were proposed: a detailed model (DM) and a hybrid model (HM). The former contains the exact representation of all power electronics equipment and is suitable for very detailed analyses with large bandwidth considerations. The latter is based on new proposed switched equivalent circuits and average model representations for the considered equipment and controllers. It allows for larger simulation time steps (up to 50 μ s), hence considerably reducing computation times, and addresses simulations in which very high frequency components can be neglected and/or averaged. A comparison was also made to demonstrate and confirm the accuracy of the HM model against its former DM representation.

Finally, the proposed model was validated against field measurements of a real wind turbine of similar type. Specific tests were conducted with focus on the FRT-capabilities. In general, a good match was obtained, confirming that the proposed generic EMT-type wind turbine model contains the required level of details to provide adequate and sufficiently accurate performance to support EMT power system studies.

TABLE III
WIND TURBINE SG PARAMETERS

Parameter	Name	Value	Unit
Pgen_nom	Nominal power	2	MVA
Vgen_nom	Nominal stator phase-to-phase voltage	830	V
fgen_nom	Nominal stator frequency	10.8	Hz
ifngen_nom	Nominal excitation current	31.7	A
Rs_gen	Stator resistance per phase	0.0726	pu
Ll_gen	Stator leakage inductance	1.3790	pu
Llmd_gen	Direct-axis magnetizing inductance	1.9701	pu
Llmq_gen	Quadrature-axis magnetizing inductance	1.9701	pu
Rf_gen	Field resistance	0.0102	pu
Lffd_gen	Field leakage inductance	0.0167	pu
Hgen_gen	Inertia coefficient	6.7	s
p_gen	Pole pairs	36	-

TABLE IV
WIND TURBINE FULL CONVERTER PARAMETERS

Parameter	Name	Value	Unit
Rs	Diode and IGBT's snubber resistance	0.1	$\text{m}\Omega$
Ron	Diode and IGBT's conducting resistance	0.1	$\text{m}\Omega$
C1	Vdc1 capacitance	50	mfF
Rboost	Boost reactor resistance	10	$\text{m}\Omega$
Lboost	Boost reactor inductance	100	mH
Rchopper	Chopper resistance	0.15	Ω
C2	Vdc2 capacitance	300	mfF
L1_filter	L1 output filter inductance	150	μH
Rd_filter	Damping circuit output filter resistance	0.025	Ω
Ld_filter	Damping circuit output filter inductance	15	mH
L2_filter	L2 output filter inductance	5	μH

TABLE V
WIND TURBINE CONTROL PARAMETERS

Parameter	Name	Value	Unit
Tau_oref	Time constant of wref filter	10	s
Vdc1_kp	Vdc1 proportional gain	0.75	-
Vdc1_ki	Vdc1 integrator gain	0.075	s^{-1}
f_cut	Cut-off freq. of measurement filter	10	kHz
zeta	Damping factor of measurement filter	0.7071	-
Kp_pll	PLL proportional gain	0.1775	-
Ki_pll	PLL integrator gain	21.3	s^{-1}
Tau_Vdc2	Time constant of Vdc2 meas. filter	33.334	ms
Vdc2_kp	Vdc2 controller proportional gain	10	-
Vdc2_ki	Vdc2 controller integrator gain	75	s^{-1}
Tau_Qref	Time constant of Qref-filter	33.334	ms
Tau_Qmeas	Time constant of Qmeas-filter	33.334	ms
Q_kp	Q-control proportional gain	0.001	-
Q_ki	Q-control integrator gain	0.035	s^{-1}
I_band	Current control tolerance band	0.017	pu

APPENDIX

The following tables contain the parameters for the proposed and validated generic 2 MW wind turbine model.

REFERENCES

- [1] IRENA, Renewable Energy Statistics 2016, The International Renewable Energy Agency, Abu Dhabi 2016.
- [2] Hydro-Québec TransÉnergie, “Transmission provider technical requirements for the connection of power plants to the Hydro-Québec transmission system,” Hydro-Québec TransÉnergie, Feb. 2009. [Online]. Available: http://www.hydroquebec.com/transenergie/fr/commerce/pdf/exigence_raccordement_fev_09_en.pdf.
- [3] C. W. G. C4.601, “Modeling and dynamic behavior of wind generation as it relates to power system control and dynamic performance,” 2007.

- [4] *Wind Turbines - Part 27-1: Electrical Simulation Models - Wind Turbines*, IEC Standard 61400-27-1, ed. 1, 2015. [Online]. Available: <https://collections.iec.ch/std/series/iec61400-27-1%7Bed1.0%7Den.nsf/doc.xsp>
- [5] WECC, “Type 3 Wind Turbine Generator Model - Phase II,” Jan. 23, 2014. [Online]. Available: <https://www.wecc.biz/Reliability/WECCType3WindTurbineGeneratorModel-PhaseII012314.pdf>.
- [6] WECC, “Type 4 wind turbine generator model - Phase II,” Jan. 23, 2014. [Online]. Available: <https://www.wecc.biz/Reliability/WECCType4WindTurbineGeneratorModel-PhaseII012313.pdf>.
- [7] R. Gagnon *et al.*, “Hydro-Québec strategy to evaluate electrical transients following wind power plant integration in the Gaspésie transmission system,” *IEEE Trans. Sustain. Energy*, vol. 3, no. 4, pp. 880–889, Oct. 2012.
- [8] L. Fan, C. Zhu, Z. Miao, and M. Hu, “Modal analysis of a DFIG-based wind farm interfaced with a series compensated network,” *IEEE Trans. Energy Convers.*, vol. 26, no. 4, pp. 1010–1020, Dec. 2011.
- [9] A. Ostadi, A. Yazdani, and R. K. Varma, “Modeling and stability analysis of a DFIG-based wind-power generator interfaced with a series-compensated line,” *IEEE Trans. Power Deliv.*, vol. 24, no. 3, pp. 1504–1514, Jul. 2009.
- [10] I. Vieto and J. Sun, “Impedance modeling of doubly-fed induction generators,” in *Proc. 17th Eur. Conf. Power Electron. Appl. (EPE'15 ECCE-Europe)*, 2015, pp. 1–10.
- [11] U. Karaagac, H. Saad, J. Peralta, and J. Mahseredjian, “Doubly-fed induction generator based wind park models in EMTP-RV,” Apr. 2015, *Polytechnique Montréal*, Research Report.
- [12] R. Gagnon, “SimScape Power system examples: wind farm—DFIG detailed model,” MathWorks Matlab2016a, 2016. [Online]. Available: <https://de.mathworks.com/help/physmod/sps/examples/wind-farm-dfig-detailed-model.html>.
- [13] U. Karaagac, J. Mahseredjian, H. Saad, J. Peralta, and L. D. Bellomo, “Simulation models for wind parks with variable speed wind turbines in EMTP-RV,” Apr. 2015, *Polytechnique Montréal*, Research Report.
- [14] R. Gagnon and J. Brochu, “Simscape power systems examples: wind farm—synchronous generator and full scale converter (Type 4) detailed model,” MathWorks Matlab2016a, 2016. [Online]. Available: <https://de.mathworks.com/help/physmod/sps/examples/wind-farm-synchronous-generator-and-full-scale-converter-type-4-average-model.html>.
- [15] X. Yuan, F. Wang, D. Boroyevich, R. Burgos, and Y. Li, “DC-link voltage control of a full power converter for wind generator operating in weak-grid systems,” *IEEE Trans. Power Electron.*, vol. 24, no. 9, pp. 2178–2192, Sep. 2009.
- [16] H. Huang, C. Mao, J. Lu, and D. Wang, “Small-signal modelling and analysis of wind turbine with direct drive permanent magnet synchronous generator connected to power grid,” *IET Renew. Power Gener.*, vol. 6, no. 1, p. 48–58, Jan. 2012.
- [17] I. Vieto, H. Liu, S. Rogalla, and J. Sun, “On the potential of subsynchronous resonance of voltage-source converters with the grid,” in *Proc. 5th Solar and 14th Wind Integr. Workshop*, Brussels, Belgium, Oct. 2015, pp. 438–443.
- [18] *Establishing a Network Code on Requirements for Grid Connection of Generators*, Official Journal of the European Union—Legislation: Commission Regulation (EU) 2016/631, Apr. 14, 2016.
- [19] TAB-HS-Germany, “VDE-AR-N 4120:2015-01 Technical requirements for the connection and operation of customer installations to the high-voltage network (TCC high-voltage),” 2016. [Online]. Available: <https://shop.vde.com/en/vde-ar-n-41202015-01-technical-requirements-for-the-connection-and-operation-of-customer-installations-to-the-high-voltage-network-tcc-high-voltage>
- [20] National-Grid (UK), “The Grid Code,” 2013. [Online]. Available: <https://www.nationalgrid.com/sites/default/files/documents/8589935310-Complete%20Grid%20Code.pdf>
- [21] ONS - Operador Nacional do Sistema Elétrica (Brazil), “Submódulo 3.6—Requisitos técnicos mínimos para a conexão às instalações de transmissão,” [Online]. Available: [http://www.ons.org.br/%2FProcedimentosDeRede%2FM%C3%B3dulos%203%2FSubm%C3%B3dulos%203.6_Rev_1.1.pdf](http://www.ons.org.br/%2FProcedimentosDeRede%2FM%C3%B3dulos%203%2FSubm%C3%B3dulos%203.6%2FSubm%C3%B3dulos%203.6_Rev_1.1.pdf)
- [22] T. Ackermann, Ed., *Wind Power in Power Systems*. Chichester, UK: Wiley, 2012.
- [23] R. Gasch and J. Twele, Eds., *Wind Power Plants*. Berlin, Heidelberg, Germany: Springer, 2012.
- [24] A. Yazdani and R. Iravani, *Voltage-Sourced Converters in Power Systems*. Hoboken, NJ, USA: Wiley, 2010.
- [25] M. Fischer and M. Schellschmidt, “Fault ride through performance of wind energy converters with FACTS capabilities in response to up-to-date German grid connection requirements,” in *Proc. IEEE/PES Power Syst. Conf. Expo. (PSCE)*, 2011, pp. 1–6.
- [26] V. Diedrichs, A. Beekmann, K. Busker, S. Nikolai, and S. Adloff, “Control of wind power plants utilizing voltage source converter in high impedance grids,” in *Proc. IEEE Power Energy Soc. Gen. Meet.*, 2012, pp. 1–9.
- [27] M. Fischer, A. Mendonca, S. Engelken, and N. Mihov, “Operational experiences with inertial response provided by type 4 wind turbines,” *IET Renew. Power Gener.*, vol. 10, no. 1, pp. 17–24, Jan. 2016.
- [28] H. Emanuel, M. Schellschmidt, and I. Mackensen, “Asymmetrical Current Injection - Testing and certification for new German requirements,” in *Proc. 15th Int. Workshop Large Scale Integr. Wind Power Power Syst.*, Vienna, Austria, Nov. 2016, pp. 434–438.
- [29] R. W. Erickson and D. Maksimović, *Fundamentals of Power Electronics*. Boston, MA, USA: Springer, 2001.
- [30] R. N. Beres, X. Wang, M. Liserre, F. Blaabjerg, and C. L. Bak, “A review of passive power filters for three-phase grid-connected voltage-source converters,” *IEEE J. Emerg. Sel. Top. Power Electron.*, vol. 4, no. 1, pp. 54–69, Mar. 2016.
- [31] R. N. Beres, X. Wang, F. Blaabjerg, M. Liserre, and C. L. Bak, “Optimal design of high-order passive-damped filters for grid-connected applications,” *IEEE Trans. Power Electron.*, vol. 31, no. 3, pp. 2083–2098, Mar. 2016.
- [32] P. Giroux, “Simscape power systems: Power converter modeling techniques,” MathWorks Matlab2016a, 2016.
- [33] C. Langlois, M. Asmine, M. Fischer, and S. Adloff, “On-site under voltage ride through performance tests-assessment of ENERCON wind energy converters based on Hydro-Québec TransÉnergie requirements,” in *Proc. IEEE Power and Energy Soc. Gen. Meet.*, 2012, pp. 1–8.

Aramis Schwanka Trevisan (SM’15) first received his degree in electrical engineering from the Federal University of Paraná, Brazil, and Diplom-Ingenieur degree (equivalent to M.Sc.) from the Leibniz University of Hannover, Germany. Since 2015, he has been working toward the Ph.D. degree in electrical engineering at the Polytechnique Montréal, Montreal, Canada. He joined the research and development team of ENERCON (WRD GmbH) in 2012 and has been since involved in many research and development projects addressing new grid technologies, grid integration, and modeling of ENERCON’s wind turbines and products.

Amgad A. El-Deib received the B.Sc. and M.Sc. degrees from Cairo University, Giza, Egypt, in 2002 and 2005, respectively, and the Ph.D. degree from the University of Toronto, Toronto, Canada, in 2010. From 2010 to 2012, he worked as a Power System Engineer with Hatch Limited, Toronto. Afterward, he joined the wind turbine manufacturer ENERCON in the research and development department focusing on power system integration of wind power plants. In 2015, he joined Cairo University as an Assistant Professor. His research interests include modeling and control of power electronics in power systems.

Richard Gagnon received the B.Sc. degree in physics engineering, and the M.Sc. and Ph.D. degrees in electrical engineering from Université Laval, Québec, Canada, in 1990, 1992, and 1997, respectively. From 1996 to 2001, he was a Professor of electrical engineering with the Université du Québec à Rimouski, Rimouski, Canada. Since 2001, he has been a Research Engineer with IREQ (Hydro-Québec’s Research Institute), Varennes, Canada. His research interests include modeling and simulation of power systems. Prof. Richard Gagnon is a registered Professional Engineer in the province of Québec.

Jean Mahseredjian (FM’13) received the Ph.D. degree from Polytechnique Montréal, Canada, in 1991. From 1987 to 2004, he was with IREQ (Hydro-Québec) working on research and development activities related to the simulation and analysis of electromagnetic transients. In December 2004, he joined the Faculty of Electrical Engineering at Polytechnique Montréal.

Martin Fecteau received the B.Sc.A. degree in electrical engineering from Université Laval, Québec City, in 2001. Since 2002, he has been working with Hydro-Québec TransÉnergie in the System Studies group of the Transmission System Planning Department, where he has been involved in several studies concerning wind farm integration, SSCI, EMTP modeling, protection, and SPS. Mr. Fecteau is a member of the IEEE Power Engineering Society and a registered professional engineer in the Province of Québec.